Meso-Scale Simulations of Solid–Liquid Flow and Strategies For Meso–Macro Coupling†

J. J. Derksen*

Chemical & Materials Engineering Department, University of Alberta, Edmonton, AB, T6G 2G6, Canada

Solid–liquid flows span a large parameter space, with dimensionless coordinates such as Stokes numbers, the solids volume fraction, the density ratio between the phases, and Reynolds numbers (e.g., associated with the continuous phase flow). We are interested in systems with appreciable inertia effects—that is, nonzero Stokes and Reynolds numbers—having density ratios of the order of one and solids volume fractions of order 0.1. In such flows, direct numerical simulations are desired to reveal the relevant interactions. The resolution required for DNS limits the size of the systems that we are able to simulate to the meso-scale. In this article, examples of direct simulations based on the lattice-Boltzmann method of dense solid–liquid flows are presented, along with suggestions as to how to use their results at the macro-scale.

Keywords: multiphase flow, suspensions, direct numerical simulation, lattice-Boltzmann, mesoscopic modelling

INTRODUCTION

Solid–liquid suspensions are abundant in natural and engineered systems. In general, solid–liquid flows span a large parameter space, with dimensionless components such as the Stokes number, the solids volume fraction, the density ratio between the phases, and Reynolds numbers (e.g., associated with the continuous phase flow). Our interest in large-scale industrial multiphase flows implies that we have systems with appreciable inertia effects—that is, nonzero Stokes and Reynolds numbers—having density ratios of the order of one and solids volume fractions of order 0.1. In such suspensions many assumptions that ease the life of the computational researcher do not hold, and direct simulations—including full resolution of the solid–liquid interfaces—are desired to reveal the relevant interactions at the scale of the particles.

This necessarily limits the size of the systems that we are able to simulate; they typically contain up to a thousand particles. In this article, the scales related to particle size and multi-particle interaction will be termed meso-scales, and our direct simulations are meso-scale simulations. Next to the ambition to fully resolve meso-scale phenomena, we are faced with the issue as to how to incorporate insights gained at the meso-scale in macro-scale modelling approaches (meso-to-macro coupling). In the opposite direction (macro-to-meso), the meso-scale systems need to be agitated (energised) in a manner that realistically represents the energy input that in many practical processes comes from the macro-scale; think of agitation by impellers, jets, distributor plates and pumps.

Given the variety of multiple-scale interactions in industrial multiphase flow systems there is, to our knowledge, not a general methodology or framework for establishing the macro–meso coupling. In this article we present a few examples of meso-scale simulations in the area of liquid–solid suspensions, and also show how their results could be incorporated in macroscopic flow and transport modelling.

The article is organised in the following manner: First, we give a short overview of our computational methodology which is largely based on the lattice-Boltzmann method for solving the flow of the interstitial liquid. We then briefly describe methods for generating homogeneous, isotropic turbulence as a basic way to excite meso-scale systems. Subsequently applications will be discussed. They comprise turbulence-particle interaction, flow-induced forces in agglomerates and fibres, liquid–solid fluidisation, and scalar mixing in solid–liquid flow.

†Series of featured articles on Multiphase CFD for Industrial Processes
*Author to whom correspondence may be addressed.
E-mail address: jos@ualberta.ca
Can. J. Chem. Eng. 90:795–803, 2012

DOI 10.1002/cjce.21629
Published online 27 December 2011 in Wiley Online Library (wileyonlinelibrary.com).

COMPUTATIONAL APPROACH

Lattice-Boltzmann Method

The continuous phase (liquid) flow we solve with the lattice-Boltzmann method (LBM). For flows in complexly shaped domains and/or with moving boundaries, this method has proven its usefulness (see e.g., the review article by Chen and Doolen, 1998). In the LBM, the computational domain is discretised into a number of lattice nodes residing on a uniform cubic grid. Fluid parcels move from each node to its neighbours according to prescribed rules. It can be proven by means of a Chapman–Enskog expansion that, with the proper grid topology and collision rules, this system obeys, in the low Mach number limit, the incompressible Navier–Stokes equations (Chen and Doolen, 1998; Succi, 2001). The specific implementation used in our simulations has been described by Somers (1993); it is a variant of the widely used Lattice BGK scheme to handle the collision integral (e.g., see Qian et al., 1992). We use the scheme due to Somers, as it manifests a more stable behaviour at low viscosities when compared to LBGK.

Liquid–Solid Coupling

In the lattice-Boltzmann flow field spherical (usually monosized) solid particles are suspended. The solid–liquid interfaces are fully resolved. The fluid flow and the motion of the spheres are coupled by demanding that at the surface of each sphere the fluid velocity matches the local velocity of its surface (that is the sum of the translational velocity $\mathbf{v_p}$ and $\Omega_\mathbf{p} \times (\mathbf{r} - \mathbf{r_p})$ with $\Omega_\mathbf{p}$ the angular velocity of the sphere, $\mathbf{r_p}$ the center position of the sphere, and $\mathbf{r}$ a point on its surface). In the forcing scheme (aka immersed boundary method) that is applied here this is accomplished by imposing additional forces on the fluid at the surface of the solid sphere (which are then distributed to the lattice nodes in the vicinity of the particle surface). The details of the implementation can be found elsewhere (Goldstein et al., 1993; Derksen and Van den Akker, 1999; Ten Cate et al., 2002). The collection of forces acting on the fluid at the sphere's surface and its interior is subsequently used to determine the hydrodynamic force and torque acting on the sphere (*action* $= -$*reaction*) (Derksen and Sundaresan, 2007).

In our simulations, the radius of each spherical particle is specified and input radius refers to this radius scaled by the lattice spacing. In the LBM simulations, as the spherical particle is represented by forces that are confined to a cubic grid, the input radius does not reflect the actual radius of the particle. A calibration procedure to estimate the effective radius of this object (commonly referred to as the hydrodynamic radius) was introduced by Ladd (1994). We apply his scheme to estimate the hydrodynamic radius of the particles. The hydrodynamic radius is recognised as a and is given in lattice units. In our work radii in the range $a = 6$–12 are used. Typically the input radius turns out to be some 10% smaller than the hydrodynamic radius (Ten Cate et al., 2002).

In multiple-sphere systems when two particles are at close proximity, with their separation being of the order of or less than the lattice spacing, the hydrodynamic interaction between them will not be properly resolved by the lattice. Therefore, we explicitly impose lubrication forces on the particles, in addition to the hydrodynamic forces stemming from the LBM. We use the procedure developed by Nguyen and Ladd (2002) to smoothly make the transition between resolved and unresolved hydrodynamic interactions.

In addition to interactions via the liquid, spherical particles undergo direct interactions, mostly hard-sphere. If the motion of the spheres is constrained (such as with fibres built of strings of spheres) we—for reasons of computational efficiency—apply soft-sphere interactions.

Homogeneous, Isotropic Turbulence

A typical way to agitate our meso-scale systems is by generating turbulence in fully periodic, three-dimensional domains. Adding particles to the domains allows us to study the (two-way) coupling of solid and liquid motion. So far mainly homogeneous isotropic turbulence (HIT) has been considered in our work. HIT is, for example, characterised by its root-mean-square velocity u_{rms} and a Kolmogorov length scale $\eta_\mathrm{K} = (\nu^3/\bar{\varepsilon})^{1/4}$ with $\bar{\varepsilon}$ the volume and time averaged dissipation rate (which in steady state in a fully periodic domain equals energy input) and ν the kinematic viscosity of the liquid. If solids are added, the relevant dimensionless numbers are then based on the radius of the spherical particles involved: a/η_K and (if $a/\eta_\mathrm{K} \geq 1$ so that the turbulence scales interfere with the sphere size) $Re_{\mathrm{rms}} = ((u_{\mathrm{rms}}a)/\nu)$.

We have been using two different strategies to make HIT. One is based on random forcing and was introduced by Alvelius (1999) in the context of spectral methods, later adapted for the lattice-Boltzmann method by Ten Cate et al. (2006). This strategy has the advantages that the power input can be controlled accurately, and that it allows for more general forms of turbulence, including anisotropy. The second strategy is linear forcing, where turbulence is sustained by a force that is proportional to the local velocity (Rosales and Meneveau, 2005). This method has the elegance of simplicity and (as a result) computational efficiency at the cost of being less general than random forcing.

CASE STUDIES

DNS of Turbulently Agitated Solid–Liquid Suspensions

With a view to applications in industrial crystallisation, Ten Cate et al. (2004) studied the motion of solid, spherical particles released in HIT. The conditions were such that (a/η_K) was of the order of 10, and Re_{rms} roughly 50. Given the solid over density ratio being approximately 1.5 the Stokes number based on u_{rms} ($St_{\mathrm{rms}} \equiv (2/9)(\rho_\mathrm{s}/\rho_\mathrm{f})Re_{\mathrm{rms}}$) is typically 15, indicating inertial particles. The statistics for particle–particle collisions (frequency, intensity) is of particular interest since attrition, that is, breakage of crystals due to collisions is an important issue in crystallisation as it directly and indirectly influences the crystal size distribution. The direct influence is obvious; the indirect influence on the size distribution is a result of breakage fragments acting as (secondary) sources of nucleation.

As is known from experimental (Elghobashi and Truesdell, 1993) as well as numerical work (Boivin et al., 1998), the presence of the particles affects the turbulence spectrum. Figure 1 shows spectra at different solids loadings. As evident from the spectra, and also from a direct look into our simulations, the spheres generate turbulence at scales comparable to and smaller than the particle diameter. This effect is a pronounced function of the solids volume fraction: the more particles, the stronger the effect. At the same time the slow (inertial) response of the solid particles reduces the fluctuations levels (damps turbulence) for smaller wavenumbers (i.e., at larger scales).

Our main interest was to quantify particle collisions, in terms of frequencies and intensities. In this respect it was revealing to study the probability density function (PDF) of the time between two collisions of a particle (as given in Fig. 2). For "long times" this

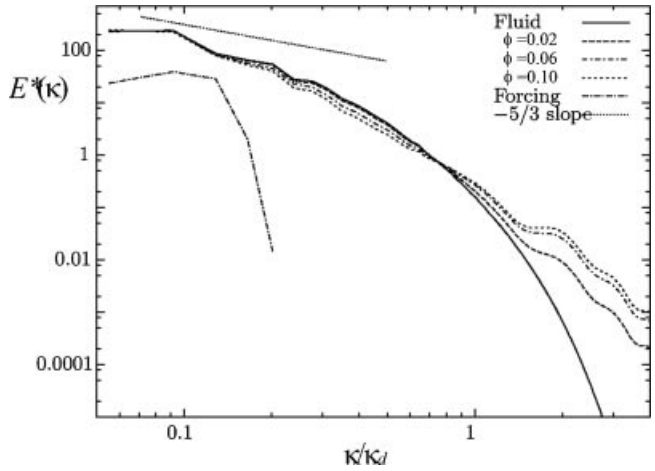

Figure 1. Energy spectra of two-phase simulations compared to the fluid-only spectrum. The wave number κ is normalised with the particle size wave number $\kappa_d = \pi/a$.

PDF is exponential indicating Poisson statistics; collisions after "long" time intervals are uncorrelated events. The slopes in Figure 2 get steeper for denser systems, that is, the average time between uncorrelated collisions gets shorter for denser systems. More interestingly, however, for "short times" the PDF shows a peak towards zero time, indicating many collisions taking place shortly after one another. Closer inspection teaches that these are correlated events: once turbulence has brought two (or more) particles in each other's vicinity they tend to cluster due to short range hydrodynamic interaction and undergo many (weak) collisions at short time intervals. Lubrication forces play a prominent role in the lifetime of the clusters. Eventually the particles in the cluster are separated when a strong enough (turbulent) eddy comes by.

In terms of macro-scale modelling, results related to collision statistics as a function of turbulence quantities and solids loading could be incorporated in (macro-scale) scale CFD/population balance simulations of crystallisation processes. Local quantities for turbulence and solids volume fraction as obtained with the CFD can be—with the help of our mesoscopic simulation results—translated in collision frequencies and intensities.

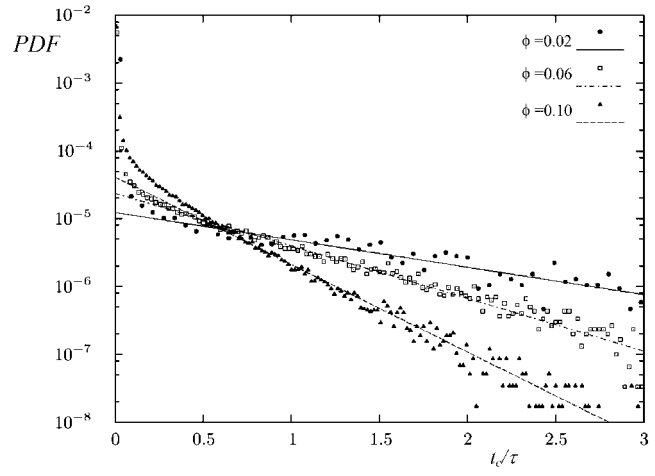

Figure 2. PDF of the time between two collisions for three solids volume fractions. The lines are linear fits of the tails of the distribution. The collision time has been made dimensionless with the Kolmogorov time scale τ.

Together with information regarding crystal strength this could be fed into a population balance model for predicting crystal breakage and (resulting) crystal size distributions.

Flow-Induced Forces in Agglomerates and Fibres

In many processes involving solid particle formation or solids handling, particles have a tendency to stick together. Sometimes agglomeration is a wanted phenomenon to effectively grow particles making separation easier. It also is a mechanism that potentially destroys a narrow particle size distribution, and as a result could deteriorate product quality. Much effort goes into preventing or promoting agglomeration, and much effort goes into repairing the harm agglomeration has done. Regardless of whether agglomeration is wanted or unwanted, it is relevant to assess the stability and the integrity of the bond holding the primary particles together. Agglomerates can break as a result of a variety of mechanisms, one of them being the flow of fluid surrounding the agglomerate: velocity gradients induce forces on and in agglomerates that could break them.

Understanding and modelling agglomerate breakage as a result of fluid flow is largely based on relatively simple concepts involving estimating shear rates and semi-empirical correlations for breakage statistics. As described in recent articles on the broader subject of population balance modelling of colloidal dispersions (Soos et al., 2006), the physics of breakage due to flow date back quite some time (Delichatsios and Probstein, 1976; Kusters, 1991), and are prone to refinement in terms of getting the (statistics of the) hydrodynamic environment of agglomerates right, and in terms of estimating the actual hydrodynamic forces in agglomerates immersed in complex flow.

As a starting point we here assess the role of some of the non-ideal factors in the flow-induced forces in agglomerates. For this we have chosen to consider the virtually simplest agglomerate possible: two equally sized spheres (radius a), rigidly constrained together at their (single) point of contact. The two spheres are touching, they have zero separation.

We release a single doublet in homogeneous, isotropic turbulence (now generated through linear forcing) and monitor the forces and torques at the point of contact needed to keep the two spheres attached. The time series are highly erratic (see the example in Fig. 3), with the fluctuation levels usually much higher than the averages. Running a number of simulations with (a/η_K) as the main variable shows an interesting scaling of the force fluctuation levels. As (a/η_K) increases, the flow around the agglomerate gets more inhomogeneous which adds to the fluctuations, see Figure 4. More details and results can be found in a recent article (Derksen, 2008a).

An extension of the above work is to consider (flexible) fibres in turbulent flow. If the fibres have a finite bending stiffness, we expect an interesting competition between turbulence bending the

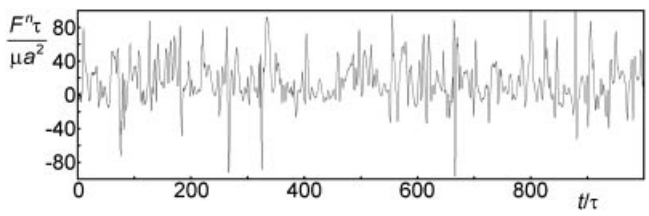

Figure 3. Time series of the flow-induced normal force at the point of contact of a sphere doublet. Time has been normalised with the Kolmogorov time scale τ.

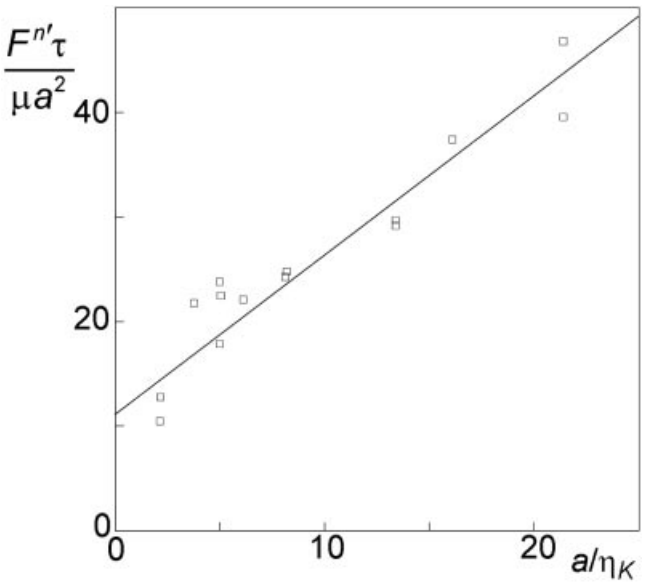

Figure 4. Root-mean-square $F^{n'}$ normal force in the sphere doublet at various turbulence conditions, characterised by the ratio (a/η_K) along with a trend line.

fibres, and stiffness trying to keep the fibres stretched. The fibres are modelled as equally sized spheres connected through rods and hinges, see Figure 5. The bending stiffness enters through a (restoring) torque that is proportional to the vector product of the vectors defining the two rods connected by the joint (see the right panel of Fig. 5): $\mathbf{T_{jm}} = -\gamma((\mathbf{j_m} \times \mathbf{j_{m+1}})/j^2)$ with γ the stiffness parameter. Some preliminary results are given in Figure 6 in terms of snapshots of the fibres bending in turbulent flow, and Figure 7 in terms of time series of the fibre-averaged bending angle. Obviously, the stiffer the fibre, the more it stays stretched in turbulent flow.

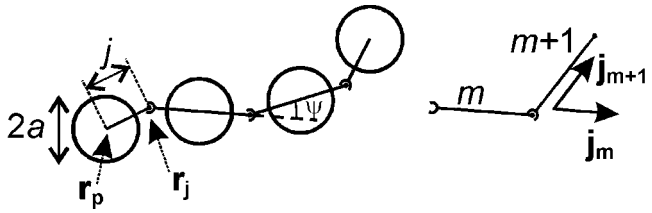

Figure 5. Definition of fibres as spheres connected through joints. Right: definition of the rod vectors $\mathbf{j_m}$.

As for the sphere doublets, we also keep track of the forces and torques required to retain the integrity of the fibres. The torque obviously increases with increasing fibre stiffness; the force is quite independent of the stiffness of the fibres, as is evident from Figure 8.

DNS of Liquid–Solid Fluidisation

Our numerical work of liquid–solid fluidisation is inspired by the experimental work due to Duru et al. (2002). They carried out an extensive study of the onset and characteristics of planar waves in relatively narrow liquid fluidised beds. Their experimental variables were the ratio of particle and fluid densities, the particle size, the fluid viscosity, the size ratio (particle diameter divided by tube diameter) and the average particle volume fraction (which was controlled by the superficial velocity of the fluidising liquid). Figure 9 shows a typical experimental result obtained by them: a space–time plot of the solids volume fraction. Clearly visible are regions of low particle volume fraction ("voids") that travel with a well-defined speed in the vertical (z) direction.

Here we directly simulate one-dimensional travelling waves such as those shown in Figure 9. The specific experiments that we selected from Duru et al. (2002) had particles with $a = 342\ \mu$m and a density ratio $(\rho_s/\rho_f) = 4.1$. In order to keep the computations affordable, we restricted our simulations to a fully periodic

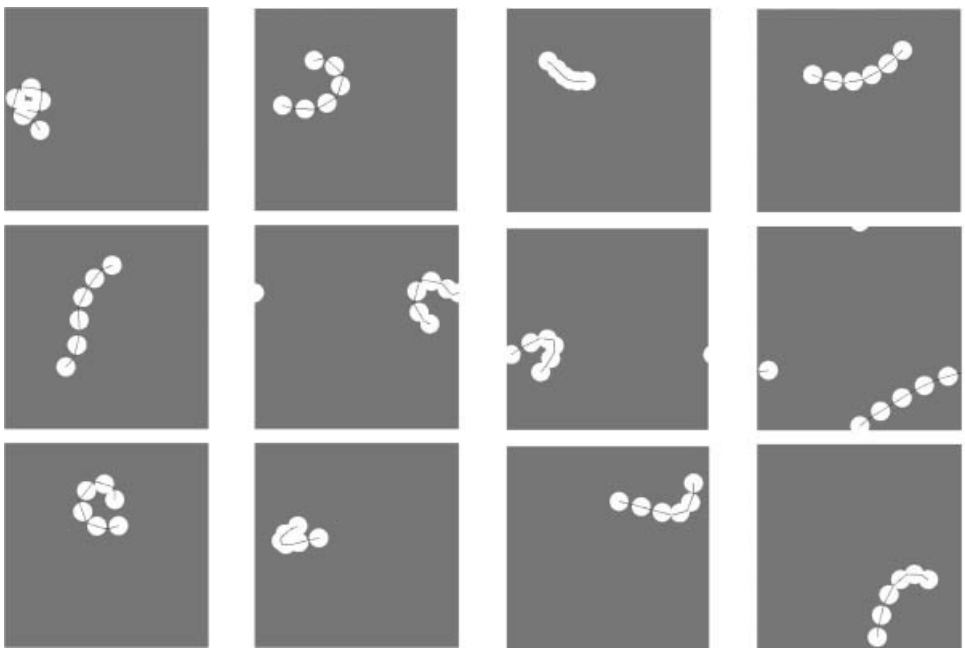

Figure 6. Side views of fibres in the 128^3 periodic domain, three snapshots per case. From left to right: increasing bending stiffness γ (see text): $(\gamma/(12\pi\nu\rho a^2 u_{rms})) = 0$, 1.78, 14.2, 56.8.

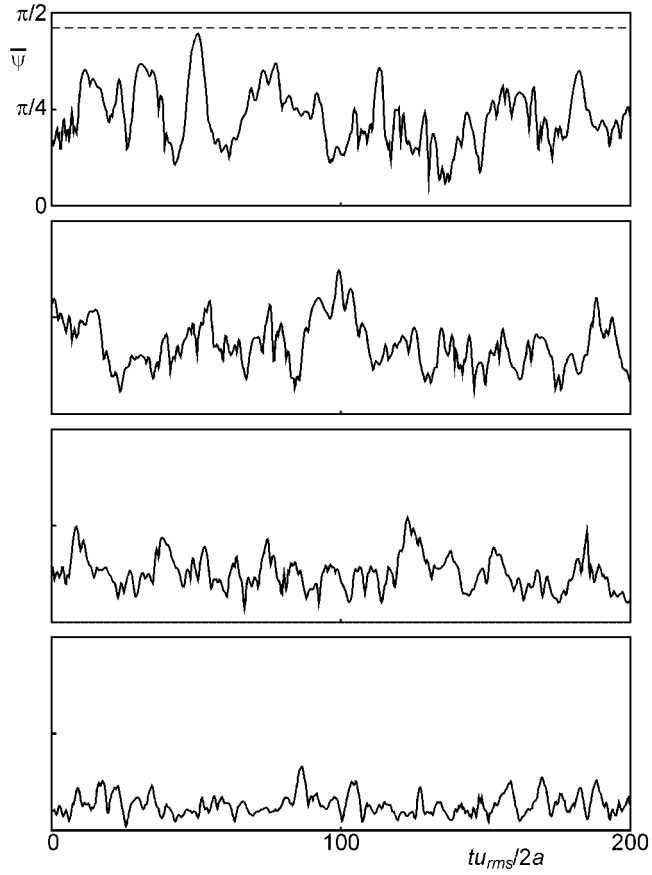

Figure 7. Time series of the fibre-averaged angle $\bar{\psi}$ with from top to bottom increasing bending stiffness ($\gamma/(12\pi\nu\rho a^2 u_{\text{rms}})) = 0$, 1.78, 14.2, 56.8. The dashed line in the upper panel represents ψ_{max}, that is, the fibre-averaged angle of a fully curled up fibre.

three-dimensional domain. Since we wish to simulate one-dimensional travelling waves, we suppress the onset of secondary instabilities by choosing the lateral dimensions to be small (typically $12a$).

A homogeneous bed was first created by placing a set of nonoverlapping spheres randomly in space in the periodic domain. At the start of the simulation, the velocities of the particles and the fluid were set to zero. At $t = 0$, gravity and the body force on the fluid were turned on. As the lateral dimensions of the domain are small, there is very little opportunity for any persistent lateral structure to evolve, but one can readily see nonuniform structures that travel in the direction of the mean fluid flow. This is illustrated in Figure 10, which shows a series of snapshots taken at an arbitrary vertical cross section of the periodic domain. The system develops a wave structure in a time span of the order of a^2/ν. A region of lower particle volume fraction, henceforth referred to as "void", travels in the direction opposite to gravity (i.e., the positive z-direction). Outside the void, the particle volume fraction is significantly higher than the average value $\bar{\phi}$. Above the void, particles detach from the dense region, then "rain" through the void, and subsequently collect on the dense region below the void.

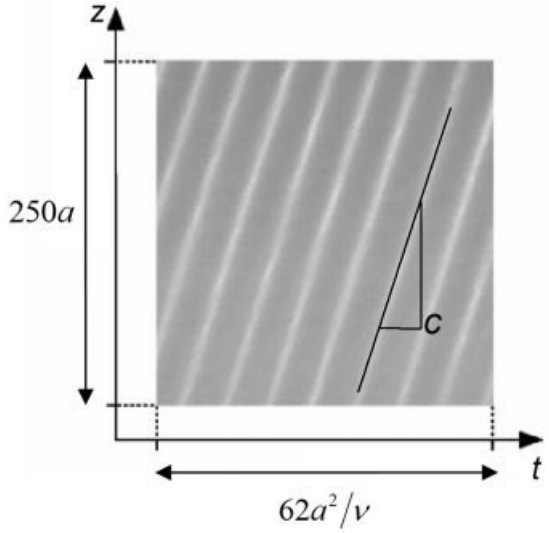

Figure 9. Experimental space-time plot of the solids volume fraction at an average solids volume fraction of $\bar{\phi} = 0.540$. The wave speed c can be deduced from the slope of the light lines representing the void regions. Reprinted from Duru et al. (2002).

The simulated wave was averaged over the horizontal directions (x and y), and represented in a space–time plot similar to the experimental ones, as an example at $\bar{\phi} = 0.488$ see Figure 11. The dimensionless wave speed $\tilde{c} = (ca)/\nu$ (with c being the dimensional wave speed) extracted from Figure 11 is 16.6. The error margin in determining $\tilde{c}$ from the simulation results was estimated as ± 1. For the comparable experimental system Duru et al. (2002) measured a dimensionless wave speed of 14 (± 1).

The liquid-particle system transfers momentum through a variety of mechanisms: particle and fluid streaming motion

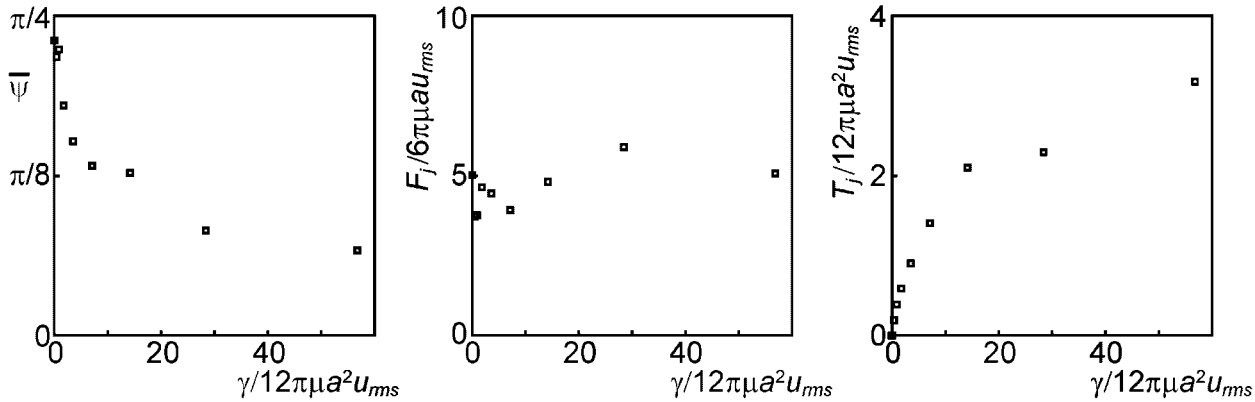

Figure 8. Time-averaged, fibre-averaged angle, absolute joint force, and absolute joint torque (from left to right) as a function of the fibres' bending stiffness γ.

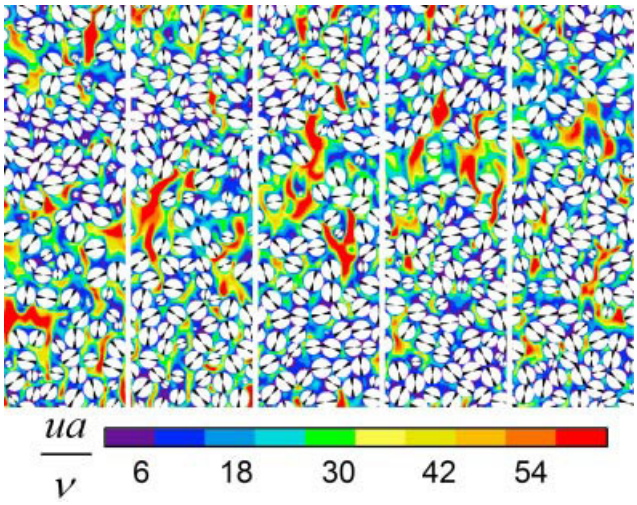

Figure 10. Cross section through the simulated liquid–solid field with $\bar{\phi} = 0.505$ at various moments in time. Colours indicate liquid velocity magnitude. [Color figure can be seen in the online version of this article, available at http://onlinelibrary.wiley.com/journal/10.1002/(ISSN)1939-019X]

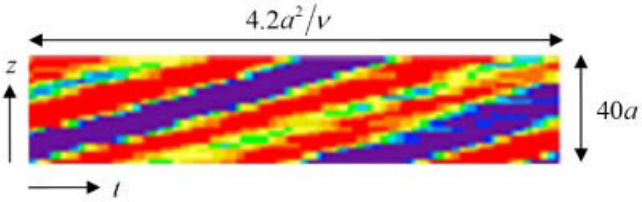

Figure 11. Space (vertical) versus time plot of the solids volume fraction for a simulation at $\bar{\phi} = 0.488$. [Color figure can be seen in the online version of this article, available at http://onlinelibrary.wiley.com/journal/10.1002/(ISSN)1939-019X]

(streaming stresses), particle–particle collisions (collisional stress), particle–particle interaction through lubrication forces, and fluid-phase viscous stresses. The wave clearly induces anisotropy. As an example, we show in Figure 12 (left panel) the three components of the collisional normal stress. As expected, the two lateral components (xx and yy) are approximately equal to one another, and the axial component (zz) differs appreciably from the other two. The effects of particle volume fraction are clearly visible in the stress profiles. The collisional stress is much lower in the void region than in the dense plug.

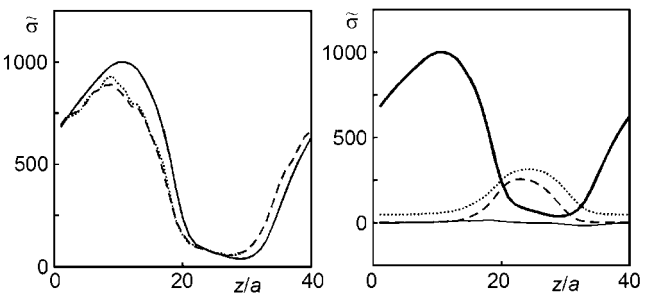

Figure 12. Dimensionless stress $\tilde{\sigma} = \sigma(a^2/(\rho_f \nu^2))$ as a function of height for $\bar{\phi} = 0.505$. Left: the three components of the collisional normal stress with the drawn line the zz component. Right: thick, drawn line: collisional stress; thin drawn line: stress due to lubrication; dotted line: fluid streaming stress; dashed line: particle streaming stress.

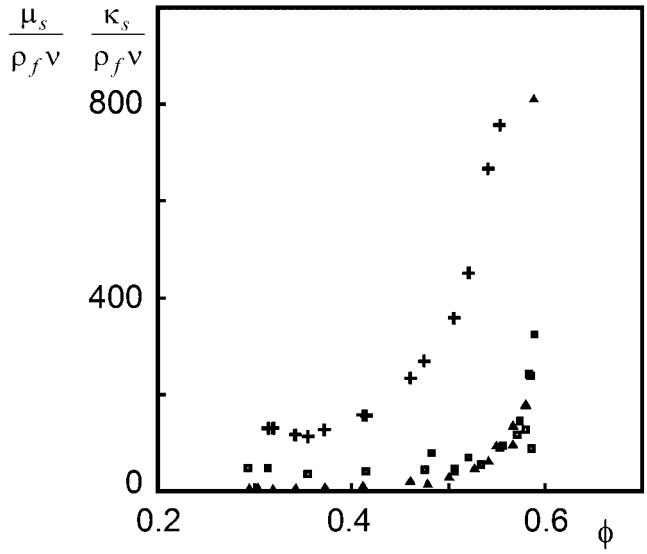

Figure 13. Particle-phase viscosity as a function of solids volume fraction. The squares (triangles) denote the shear viscosity in the compaction (dilation) branch. The plusses are bulk viscosity estimates.

The most important zz-stresses are presented in Figure 12 (right panel). Collisions are largely responsible for the particle phase stress in the parts of the flow that have a high particle volume fraction. In the void, fluid and particle streaming stress are significant and of comparable magnitude. Lubrication only plays a modest role. The fluid-phase viscous normal stresses (not shown in Fig. 12) are negligible.

The results have been further analysed in terms of the solids phase bulk and shear viscosity (Derksen and Sundaresan, 2007). Given the expansion and compression of the solids phase in the wave, and the significant stresses related to the compaction part, the bulk viscosity is significant and in general is higher than the shear viscosity, see Figure 13.

Analysis of its results towards two-fluid closure of multiphase flow is a primary motivation for performing direct simulations as described above. Two-fluid closure requires expressions that relate, for example, solids-phase viscosity with the properties of the granular system (such as local solids volume fraction and granular temperature). Our mesoscale simulations can directly assess the quality of such expressions given the availability of both the input and the output parameters in the simulations. Next to solids phase stress closure (as touched upon here in terms of solids phase viscosities), also closures for inter-phase momentum transfer (drag as a function of solids volume fraction and potentially fluctuating quantities) have been considered (Derksen and Sundaresan, 2007).

Scalar Mixing by Granular Particles

The fluctuations and inhomogeneities in fluidisation are considered helpful in mixing the solids phase. If and to what extent the motion of the solids support scalar mixing in the continuous phase is less clear. So far notions regarding this are largely based on empirical dispersion models as they can be found in, for example, the monograph by Levenspiel (1962) and references therein. Interpretation of experimental results on, for example, gas mixing in fluidised beds (e.g., Al-Sherehy et al., 2004) would benefit from a more fundamental understanding of the contribution of solids to scalar dispersion.

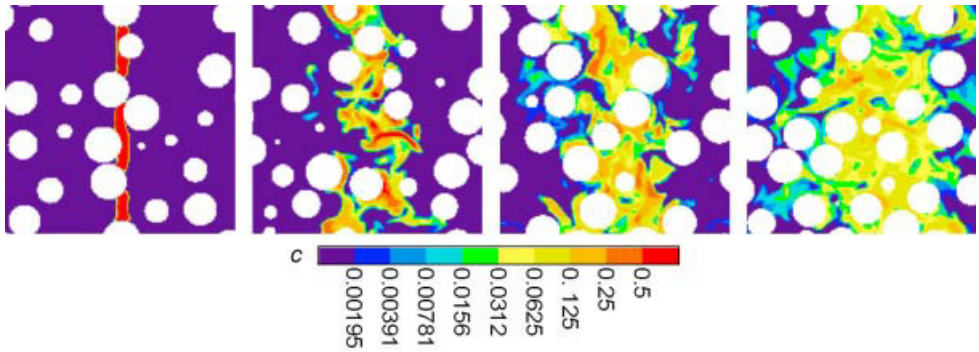

Figure 14. Snapshots of concentration contours in *xz* cross sections through the cubic domain. The white disks represent the particles that all have the same size but different distance to the plane of cross section. $\bar{\phi} = 0.30$ and $Re_g = 104$ at (from left to right) $(t\sqrt{T_g}/2a) = 0.05$, 1.96, 3.88, and 5.79 respectively. [Color figure can be seen in the online version of this article, available at http://onlinelibrary.wiley.com/journal/10.1002/(ISSN)1939-019X]

Also—in the context of CFD of turbulent disperse multiphase flows—it is quite common to apply the analogy of transport of momentum by eddies and of a scalar for estimating scalar eddy diffusion/dispersion coefficients. It is questionable if such an approach would be valid for systems with high volumetric disperse phase loadings. In dense systems turbulence can hardly develop due to the small interparticle spacings, leaving an eddy diffusivity concept without a firm physical basis.

To address and investigate the issues identified above, we here describe fully resolved numerical experiments that directly probe the spreading of a passive scalar as a result of solid particle motion. The moving particles agitate the interstitial fluid. Subsequently the flow disperses the scalar dissolved in the fluid. Goals of the simulations are to find out how the scalar spreading scales with the parameters governing the particle and fluid motion such as the granular temperature, the mean free path of the particles and the fluid's viscosity, and to propose expressions for scalar dispersion coefficients.

The systems we study numerically consist of three-dimensional periodic domains that contain solid particles and interstitial fluid. The particles move as a granular gas with a constant temperature, that is, they move ballistically through the fluid and undergo fully elastic and smooth collisions. The particles do not feel the presence of the fluid. At the fluid–solid interfaces, however, we impose a no-slip condition on the fluid. In that manner the fluid responds to the particle motion and gets agitated. Once this fluid–solid system is fully developed we release a passive scalar in the fluid phase. By solving the convection equation for the tracer with non-penetration boundary conditions at the solid surfaces, we observe how the tracer spreads by the action of the moving solid particles only.

The primary independent variables in the numerical experiments are the solids phase volume fraction ϕ, and the Reynolds number based on the granular temperature T_g of the particles $Re_g = (\sqrt{T_g}\, a)/\nu$. To limit the parameter space, we give the dissolved scalar a very high Schmidt number, that is, we set the molecular diffusivity of the passive scalar to zero. The (inevitable) numerical diffusion is minimised using a total variation diminishing (TVD) scheme in estimating convective fluxes (Harten, 1983). Since the fluid motion is one-way coupled to the (granular) motion of particles, the impact of the Reynolds number in scalar spreading is only via the (size of) the flow structures being generated, the Reynolds number affecting particle trajectories is not part of the computational picture.

We consider passive scalar transport in a fully developed flow of particles and fluid. As initial condition for the scalar concentration we give a thin *yz*-slab (with slab thickness $a/2$) of fluid a concentration $c = 1$, and the rest of the fluid $c = 0$. Subsequently we keep track of the spreading of the scalar as a result of the fluid flow induced by the solid particle motion. Typical sequences are given in Figure 14. The full, three-dimensional data is reduced to a one-dimensional scalar concentration function and subsequently (by fitting a Gaussian to the concentration function) to a single number characterising the width of the distribution as a function of time: $\sigma(t)$.

Analysing these data (also see Derksen, 2008b) shows that if σ as a function of time is scaled with "collisional" length and time scales, that is, the mean-free path (λ) of the granular gas as the characteristic length, and the inverse of the collision frequency $(1/f_c)$ as the characteristic time, the scalar spreading behaves quite universally over a wide range of solids volume fractions, see Figure 15. This analysis eventually leads to a tentative expression for the effective dispersion coefficient: $D = (1/2)\alpha\lambda^2 f_c$ with

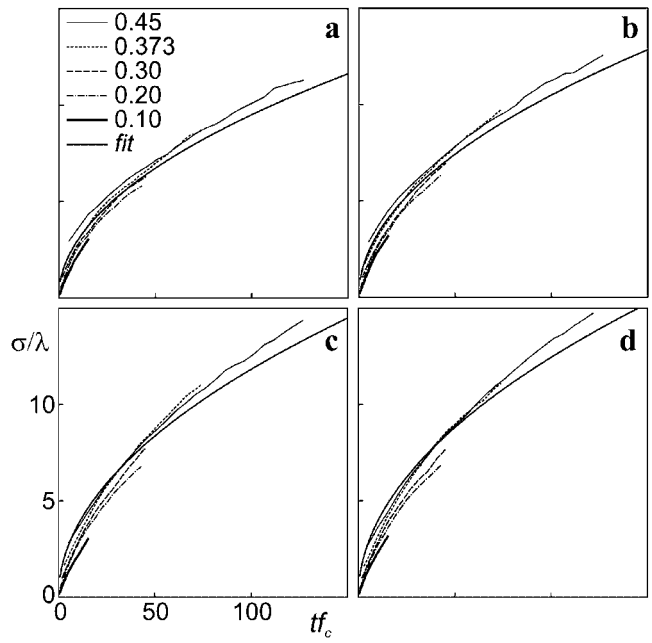

Figure 15. σ as a function of time for various solids volume fractions. Time has been scaled with the collision frequency f_c, σ with the MFP λ. Panels (a), (b), (c), and (d), respectively have $Re_g = 2.8$, 28, 104, and 280. The fit also included is the function $\sigma/\lambda = \sqrt{\alpha t f_c}$. The fitting parameter α differs per panel and is 0.9, 1.1, 1.4, and 1.5, respectively.

α a coefficient of order 1 that weakly depends on the granular Reynolds number Re_g (Derksen, 2008b). This expression for the dispersion coefficient as a function of mean-free path, collision frequency and granular Reynolds number can be used in macro-scale CFD simulations to assess the level of scalar mixing brought about by solid particle motion. For this, information regarding solids volume fraction and granular temperature obtained through the CFD is employed to estimate collision frequencies and mean-free paths.

SUMMARY AND OUTLOOK

This article presents a few case studies of mesoscopic modelling of solid–liquid flows, with underlying topics such as momentum transfer, turbulence modulation, scalar spreading, and flow-induced forces in and on agglomerates. Except for lubrication modelling, the simulations are direct, meaning that no (empirical) closures or empirical correlations, for example, forces on particles enter the simulations.

From an industrial standpoint the flow systems studied are (still) very simple: monosized spherical, solid particles in Newtonian carrier fluids. The choice for monodispersed systems is not fundamental; the simulation strategy easily allows for size distributions. The extension towards nonspherical particles would be much less straightforward. Specifically in dense systems, handling collisions of nonspherical particles would get (computationally) more complicated.

In retrospect, the reason for the relative simplicity at the mesoscale was to keep the parameter space limited. Adding complications (at the mesoscale) strongly adds to the dimensionality of the parameter space (then size distributions, particle shape characterisation, and rheological parameters would enter). It would be useful though to add complexity to the mesoscale, the challenge being to directly mimic the interactions there and for instance see how particle shape impacts momentum transfer in dense suspensions. The price to pay for this is getting less general (i.e., work towards more and more specific applications); results only apply to the specific systems of choice; the (general) link to the macro-scale would be harder to establish.

Relating with real processes and industry in this respect is essential. Zooming in on practical systems and making choices regarding the physics to be incorporated there only pays off if it helps in solving practical problems with economical and environmental impact.

From a computational perspective there is significant opportunity for increasing the size and/or complexity of the meso-scale simulations through parallelisation. The results presented above are almost exclusively based on sequential (i.e., one-cpu) computations with memory requirements per simulation in the range of 100 Mbyte to 5 Gbyte. The simulations run on Linux clusters with standard (PC) processors. Runtimes obviously depend upon the flow system characteristics. The lengthiest simulations are the ones of liquid–solid fluidisation that ran for up to 6 weeks: it first takes time for the micro-structure to develop the wave instability. Subsequent run time is needed to establish sufficiently converged flow statistics.

Parallelisation of the lattice-Boltzmann part of the computational procedure is straightforward given the local nature (only nearest neighbour interaction) of its operations. Parallelisation of the solid particle dynamics and its coupling with LBM is more complicated with the particles extending over of the order of 10 grid spacings and thus requiring more communication between cpu's in parallel runs.

NOMENCLATURE

a	sphere radius
$c, \tilde{c}$	(dimensionless) wave speed
c	scalar concentration
D	dispersion coefficient
f_c	collision frequency
$\mathbf{j_m}$	fiber joint vector
j	fiber joint length
$\mathbf{r}$	location vector
$\mathbf{r_p}$	sphere center position
t	time
T_g	granular temperature
$\mathbf{T_{jm}}$	restoring torque in fibres
u_{rms}	root-mean-square velocity
$\mathbf{v_p}$	sphere's linear velocity
α	coefficient in dispersion relation
$\bar{\varepsilon}$	average energy dissipation rate
$\phi, \bar{\phi}$	(average) solids volume fraction
γ	fiber stiffness
η_K	Kolmogorov length scale
κ	wave number
λ	mean-free path
μ	dynamic viscosity
μ_s, κ_s	solids phase shear and bulk viscosity
ν	kinematic viscosity
ρ_s, ρ_f	solids and fluid density
$\sigma, \tilde{\sigma}$	(dimensionless) stress
σ	scalar spreading width
γ	Kolmogorov time scale
$\Psi, \bar{\Psi}$	(average) fiber angle
Ω_p	sphere's angular velocity
Re_{rms}	Reynolds number based on u_{rms}
Re_g	Reynolds number based on $\sqrt{T_g}$
St_{rms}	Stokes number based on u_{rms} ($St_{rms} \equiv (2/9)(\rho_s/\rho_f)Re_{rms}$)

REFERENCES

Al-Sherehy, F., J. Grace and A.-E. Adris, "Gas Mixing and Modelling of Secondary Gas Distribution in a Bench-Scale Fluidized Bed," AIChE J. **50**, 922–936 (2004).

Alvelius, K., "Random Forcing of Three-Dimensional Homogeneous Turbulence," Phys. Fluids **11**, 1880–1889 (1999).

Boivin, M., O. Simonin and K. D. Squires, "Direct Numerical Simulation of Turbulence Modulation by Particles in Isotropic Turbulence," J. Fluid Mech. **375**, 235–263 (1998).

Chen, S. and G. D. Doolen, "Lattice Boltzmann Method for Fluid Flows," Annu. Rev. Fluid Mech. **30**, 329–364 (1998).

Delichatsios, M. A. and R. F. Probstein, "The Effect of Coalescence on the Average Drop Size in Liquid–Liquid Dispersions," Ind. Eng. Chem. Fund. **14**, 134–138 (1976).

Derksen, J. and H. E. A. Van den Akker, "Large-Eddy Simulations on the Flow Driven by a Rushton Turbine," AIChE J. **45**, 209–221 (1999).

Derksen, J. J. and S. Sundaresan, "Direct Numerical Simulations of Dense Suspensions: Wave Instabilities in Liquid-Fluidized Beds," J. Fluid Mech. **587**, 303–336 (2007).

Derksen, J. J., "Flow Induced Forces in Sphere Doublets," J. Fluid Mech. **608**, 337–356 (2008a).

Derksen, J. J., "Scalar Mixing by Granular Particles," AIChE J. **54**, 1741–1747 (2008b).

Duru, P., M. Nicolas, J. Hinch and E. Guazelli, "Constitutive Laws in Liquid-Fluidized Beds," J. Fluid Mech. **452**, 371–404 (2002).
Elghobashi, S. and G. Truesdell, "On the Two-Way Interaction Between Homogenous Turbulence and Dispersed Solid Particles. I: Turbulence Modification," Phys. Fluids **5**, 1790–1801 (1993).
Goldstein, D., R. Handler and L. Sirovich, "Modelling a No-Slip Flow Boundary With an External Force Field," J. Comp. Phys. **105**, 354–366 (1993).
Harten, A., "High Resolution Schemes for Hyperbolic Conservation Laws," J. Comp. Phys. **49**, 357–364 (1983).
Kusters, K. A., "The Influence of Turbulence on Aggregation of Small Particles in Agitated Vessel," Ph.D., Eindhoven University of Technology, Netherlands (1991).
Ladd, A. J. C., "Numerical Simulations of Particle Suspensions Via a Discretised Boltzmann Equation. Part 2. Numerical Results," J. Fluid Mech. **271**, 311–339 (1994).
Levenspiel, O., "Chemical Reaction Engineering," 2nd ed., Wiley, New York (1962).
Nguyen, N.-Q. and A. J. C. Ladd, "Lubrication Corrections for Lattice-Boltzmann Simulations of Particle Suspensions," Phys. Rev. E **66**, 046708 (2002).
Qian, Y. H., D. d'Humieres and P. Lallemand, "Lattice BGK for the Navier–Stokes Equations," Europhys. Lett. **17**, 479–484 (1992).
Rosales, C. and C. Meneveau, "Linear Forcing in Numerical Simulations of Isotropic Turbulence: Physical Space Implementations and Convergence Properties," Phys. Fluids **17**, 095106 (2005).
Somers, J. A., "Direct Simulation of Fluid Flow With Cellular Automata and the Lattice-Boltzmann Equation," Appl. Sci. Res. **51**, 127–133 (1993).
Soos, M., J. Sefcik and M. Morbidelli, "Investigation of Aggregation, Breakage and Restructuring Kinetics of Colloidal Dispersions in Turbulent Flows by Population Balance Modelling and Static Light Scattering," Chem. Eng. Sci. **61**, 2349–2363 (2006).
Succi, S., "The Lattice Boltzmann Equation for Fluid Dynamics and Beyond," Clarondon Press, Oxford (2001).
Ten Cate, A., C. H. Nieuwstad, J. J. Derksen and H. E. A. Van den Akker, "PIV Experiments and Lattice-Boltzmann Simulations on a Single Sphere Settling Under Gravity," Phys. Fluids **14**, 4012–4025 (2002).
Ten Cate, A., J. J. Derksen, L. M. Portela and H. E. A. Van den Akker, "Fully Resolved Simulations of Colliding Spheres in Forced Isotropic Turbulence," J. Fluid Mech. **519**, 233–271 (2004).
Ten Cate, A., E. Van Vliet, J. J. Derksen and H. E. A. Van den Akker, "Application of Spectral Forcing in Lattice-Boltzmann Simulations of Homogeneous Turbulence," Comp. Fluids **35**, 1239–1251 (2006).

Manuscript received September 11, 2011; revised manuscript received October 10, 2011; accepted for publication October 28, 2011.